# Structure of molten titanium dioxide

O. L. G. Alderman, L. B. Skinner, C. J. Benmore, A. Tamalonis, and J. K. R. Weber

Phys. Rev. B **90**, 094204 — Published 18 September 2014

DOI: 10.1103/PhysRevB.90.094204

# Structure of molten titanium dioxide

O.L.G. Alderman[1,2], L.B. Skinner[1,2,3], C.J. Benmore[2], A. Tamalonis[1], J.K.R. Weber[1,2]

1. Materials Development, Inc., Arlington Heights, IL 60004, USA

2. X-Ray Science Division, Advanced Photon Source, Argonne National Laboratory, Argonne, IL 60439, USA

3. Mineral Physics Institute, Stony Brook University, Stony Brook, New York, NY 11794-2100, USA

## Abstract

The x-ray structure factor of molten $TiO_2$ has been measured for the first time, enabled by the use of aerodynamic levitation and laser beam heating, to a temperature of $T$ = 2250(30) K. Ti-O coordination number in the melt is close to $n_{TiO}$ = 5.0(2), with modal Ti-O bond length $r_{TiO}$ = 1.881(5) Å, both values being significantly smaller than for the high temperature stable Rutile crystal structure ($n_{TiO}$ = 6.0, $r_{TiO}$ = 1.959 Å). The structural differences between melt and crystal are qualitatively similar to those for alumina, which is rationalized in terms of the similar field strengths of $Ti^{4+}$ and $Al^{3+}$. The diffraction data are used to generate physically and chemically reasonable structural models, which are then compared to the predictions based on various classical molecular dynamics (MD) potentials. New interatomic potentials, suitable for modelling molten $TiO_2$, are introduced, given the inability of existing MD models to reproduce the diffraction data. These new potentials have the additional great advantage of being able to predict the density and thermal expansion of the melt, as well as solid amorphous $TiO_2$, in agreement with published results. This is of critical importance given the strong correlation between density and structural parameters such as $n_{TiO}$. The large thermal expansion of the melt is associated with weakly temperature dependent structural changes, whereby simulations show that $n_{TiO}$ = 5.85(2) – (3.0(1) x $10^{-4}$)$T$ (K, 2.75 Å cut-off). The $TiO_2$ liquid is structurally analogous to the geophysically relevant high pressure liquid silica system at around 27 GPa. We argue that the predominance of 5-fold polyhedra in the melt implies the existence of as yet undiscovered $TiO_2$ polymorphs, based on lower-than-octahedral coordination numbers, which are likely to be metastable under ambient conditions. Given the industrial importance of titanium oxides, experimental and computational searches for such polymorphs are well warranted.

## I. Introduction

Titanium dioxide ($TiO_2$) is an extensively studied photocatalytic material [1] which can be used for solar energy conversion, water splitting, and degradation of organic industrial pollutants [2]. $TiO_2$ is known to demonstrate flash sintering [3-5], that is, sintering at relatively low furnace temperatures under the application of an electric field. Oxygen deficient $TiO_{2-x}$ represents a physical realization of a memristive device [6-9]. These phenomena are all related to charged defect formation in $TiO_2$, and/or to the formation of $Ti_nO_{2n-1}$ Magnéli phases. Knaup et al. [10] have recently raised the possibility of a liquid intermediate phase in both memristive device operation and during flash sintering, presumably in the form of *local* melting. Narayan [4] has proposed a mechanism for flash sintering which does indeed involve local melting at grain boundaries. The structure and properties of $TiO_2$ rich melts are also important for understanding industrial smelting of ores, e.g. ilmenite ($FeTiO_3$) [11] and in the direct electrochemical reduction of melts [12,13], e.g. for extraterrestrial resource generation .

$TiO_2$ is an end-member to several important mixed oxide systems, such as BaO-$TiO_2$, which includes the archetypal ferroelectric $BaTiO_3$, and such crystals are often derived from the liquid state, from either stoichiometric melts or fluxes. $TiO_2$ is often used as a component in melt-derived mixed oxide glasses to increase refractive index [14], or as a nucleating agent in glass-ceramics [15,16]. In terms of glass formation, $TiO_2$ is an intermediate oxide, or conditional glass former, partaking in network formation while typically not capable of being melt-quenched to form glass itself. Amorphous $TiO_2$ films have been obtained by various methods [17], such as reactive evaporation and deposition. In mixed oxide glasses Ti is often found in 5-fold coordination, including unusual [$TiO_{4+1}$] ($BaTi_2O_5$ [18]) and [$TiO_{1+4}$] ($K_2O.TiO_2.2SiO_2$ [19]) polyhedra, while in amorphous $TiO_2$, Ti is found to have an average coordination number laying between five and six [20] (dependent upon growth method). $TiO_2$ is strongly polymorphic, with at least five forms known to be metastable with respect to Rutile under ambient conditions (Fig. 1), and several high-pressure polymorphs also exist [21]. All ambient pressure polymorphs, as well as the substoichiometric Magnéli phases, contain Ti within [$TiO_6$] octahedra [22], although recent structural refinements have been used to show that one Ti site in the $TiO_2$(B) polymorph may be considered as 5-fold coordinated to oxygen [23]. The octahedral environment is also the most common in mixed oxide titanates (e.g. $BaTiO_3$), but several examples exist which contain [$TiO_4$] tetrahedra (e.g. $Ba_2TiO_4$ [24,25]), and indeed 5-fold polyhedra (e.g. β-$BaTi_2O_5$ [18]).

Recently, a trend for reduced cation-oxygen coordination in oxide melts and glasses, compared to their crystalline counterparts, has been observed [26]. The effect is typically larger for lower field strength cations, and $Ti^{4+}$ has a similar field strength to $Al^{3+}$, for which there is a large drop in average coordination number, from 6.0 to 4.4 in molten alumina [27-29], upon melting the stable Corundum form. In the case of $Al_2O_3$, several other crystalline polymorphs exist, within which Al exists in both tetrahedral and octahedral coordination to oxygen [30]. Therefore if $TiO_2$ were to exhibit a drop in coordination number from 6.0 upon melting, as predicted by recent observations [26], it can be argued that new metastable polymorphs of $TiO_2$, based on lower-than-octahedral Ti coordination, may be realized under suitable conditions.

Finally, molten $TiO_2$ potentially represents a useful structural analogue to high pressure $SiO_2$ and $GeO_2$ melts, with the structure and properties of liquid silica under pressure, in particular, bearing significant geophysical importance.

We present here the first structural measurements on the highly refractory liquid $TiO_2$, at a temperature of 2250(30) K, using a combination of aerodynamic levitation, $CO_2$ laser beam heating, and synchrotron x-ray diffraction. The measurement is used to assess the high-temperature applicability of several interatomic potential parameterizations used in classical molecular dynamics modelling, to improve upon these, and to model the temperature dependence of the liquid and amorphous state densities (thermal expansions) and structures.

## II. Theory

In a scattering experiment, the x-ray structure factor, $S(Q) - 1$, is related to the measured differential x-ray scattering cross-section, $\mathrm{d}\sigma(Q)/\mathrm{d}\Omega$, by [31]

$$S(Q)-1=\left(\frac{\mathrm{d}\sigma}{\mathrm{d}\Omega}(Q)-\sum_i c_i f_i^2(Q)-\sum_i c_i C_i(Q)\right)\left(\sum_i c_i f_i(Q)\right)^{-2} \tag{1}$$

where $c_i$ is the atomic faction of element $i$, $f_i(Q)$ the x-ray atomic form factor and $C_i(Q)$ the Compton scattering contribution. $Q = (4\pi\sin\theta)/\lambda$ is related to the scattering angle, $2\theta$, and the x-ray wavelength, $\lambda$. Written in terms of the partial structure factors, $S_{ij}(Q) - 1$, between pairs of atoms $i$-$j$,

$$S(Q)-1=\left(\sum_{i,j} c_i c_j f_i(Q) f_j(Q)\left(S_{ij}(Q)-1\right)\right)\left(\sum_i c_i f_i(Q)\right)^{-2} \tag{2}$$

and we may define the pair weighting factors

$$W_{ij}(Q)=\left(\left(2-\delta_{ij}\right)c_i c_j f_i(Q) f_j(Q)\right)\left(\sum_i c_i f_i(Q)\right)^{-2} \tag{3}$$

with $\delta_{ij}$ the Kronecker delta. $S(Q) - 1$ is related by sine Fourier transform to the total correlation function,

$$T(r)=4\pi\rho r+\frac{2}{\pi}\int_0^{Q_{\max}} Q\left(S(Q)-1\right)M(Q)\sin(rQ)\,\mathrm{d}Q\,, \tag{4}$$

where $r$ is the scalar interatomic distance, $\rho$ is the atomic number density and $M(Q)$ is the Lorch modification function [32], chosen to reduce the effects of the finite limits ($0 < Q \leq Q_{max}$) of the integral which are used in practice. The partial pair correlation functions, $t_{ij}(r) = 4\pi\rho c_j r g_{ij}(r)$, can be obtained using equation 4 and making the substitutions $T(r) \rightarrow t_{ij}(r)$, $\rho \rightarrow \rho c_j$ and $S(Q) \rightarrow S_{ij}(Q)$. Since the present high energy x-ray measurements are far from Ti and O absorption edges, dispersion terms in $f_i(Q)$ are neglected.

## III. Methods

### *A. Diffraction Measurements*

Diffraction measurements on liquid $TiO_2$ were performed at beamline 11-ID-C [33] of the Advanced Photon Source (Argonne, IL, USA). A spheroidal sample approximately 3 mm in diameter was levitated in a stream of argon (99.999% pure) flowing through a converging-diverging aerodynamic nozzle. The sample was heated from above with a partially focused $CO_2$ laser beam. The incident heating power was adjusted to control the sample temperature, which was measured with a single color pyrometer (Chino model IRCS) sighted onto the top of the sample where it was also being heated. The apparent temperature was corrected using a Wien's displacement law approximation [34] with a spectral emissivity value of 0.87 for the molten $TiO_2$ at the pyrometer wavelength of 0.85 µm. The emissivity value was estimated from the Fresnel losses for a material with a refractive index of 2.1, which is the value appropriate to amorphous $TiO_2$ [17] at the density of the melt. The pyrometer temperature was also corrected for reflection losses from a window and lens that were in the optical path. The temperature correction amounts to 86 K at the apparent measurement temperature of 2168 K, and we estimate a true temperature of 2250(30) K, with the uncertainty arising from estimated temperature gradients and fluctuations, in addition to the emissivity correction. Although there are top-to-bottom temperature gradients on the order of 100 K through the sample, by making both temperature and x-ray measurements at the top where it is heated, the temperature of the liquid being probed is relatively uniform. Structure was measured using a high energy (111.16 keV) x-ray beam with cross-section 200 µm x 400 µm horizontally incident upon the top of the sample in the region where it was heated.

The chamber housing the nozzle was open to the atmosphere at its top where the laser beam entered, while the incident and scattered x-rays passed through thin kapton windows. An area x-ray detector (Perkin Elmer XRD1621, 2048 x 2048 pixels of 200 µm x 200 µm Tl doped CsI) was used, with several offsets, perpendicular to the beam, and the patterns averaged together during the data reduction, to reduce any effects due to trapped excited states [35]. Sample to detector distance (394 mm) was calibrated using a polystyrene bead coated in polycrystalline $CeO_2$ powder, which was placed in the nozzle.

To obtain samples suitable for levitation, $TiO_2$ (Aldrich, 99.99%) was pre-melted in a water-cooled copper hearth, open to the atmosphere, using a 100 W $CO_2$ laser, and the surface tension of the melt relied upon to form roughly spherical beads. Sample contamination has been shown to be negligible by this method [36]. Discoloration of the material from white to dark grey was observed, revealing at least a small reduction in oxidation state ($Ti^{4+}$ to $Ti^{3+}$). However, mass measurements on batches of up to 122 mg could not resolve any mass loss, and a final formula $TiO_{2-x}$ with $x = 0.00(2)$, equivalent to an oxygen deficiency of 1% or less. The $TiO_2$ melt was somewhat unstable during levitation, and only short measurements were possible. The x-ray diffraction result shown here is averaged from frames collected over a total of 150 s.

To obtain information on the recovered material, separate experiments were performed at beamline 6-ID-D of the Advanced Photon Source on several finely powdered recovered beads. This was necessary due to the presence of strong preferred crystallite orientation in the solidified bead in the levitation nozzle. Powder was held within vertical, thin-walled (100 µm) kapton tubes of 2 mm internal diameter. 86.41 keV x-rays, and two separate sample to detector distances of 294 mm and 1104 mm were used, the latter yielding higher $Q$-space resolution.

The raw data were reduced from two dimensional images and corrected [35] for the effects of polarization, absorption, geometry and normalized using the programs Fit2d and PDFgetX2 [37] (GudrunX [38] was also used as a consistency check).

### *B. Liquid Density*

The density of liquid $TiO_2$ has been measured by Dingwell [39] who obtained the linear relation $\rho(T) = 3.8375 - (2.8 \times 10^{-4})T$ (in K and g $cm^{-3}$). This trend is shown in Fig. 1 and was obtained from two temperature points [39] plus an extrapolation to supercooled $TiO_2$ at 1873 K from $CaSiO_3$-$TiO_2$ pseudobinary melts containing up to 80 mol% $TiO_2$ [40]. Extrapolating the Dingwell function to 2250 K gives a liquid density of 3.21 g $cm^{-3}$ (0.0725 atoms Å$^{-3}$), which we use for our analysis.

### *C. Empirical Potential Structure Refinement*

Empirical Potential Structure Refinement (EPSR) [41] has been used to obtain a physically and chemically reasonable liquid structure, by construction, in excellent agreement with the measured x-ray structure factor and melt density. Although not unique, the EPSR model provides an estimate of the atomic structure and partial structure factors, and serves as a basis for comparison to molecular dynamics predictions. Initial Monte Carlo simulations were performed on 1032 atoms held within a cubic box of edge length 24.2 Å, set to reproduce the estimated liquid density [39] of 3.210 g $cm^{-3}$. Atoms interacted *via* Lennard-Jones (L-J) 12-6 and partial (0.5*e*) charge Coulomb terms, smoothly truncated, as described by Soper [41], using a cutoff of 12 Å. L-J parameters for oxygen were taken from Alderman *et al*. [42] ($\varepsilon_O = 0.92$ kJ $mol^{-1}$ and $\sigma_O = 3.16$ Å) and those for Ti set to $\varepsilon_{Ti} = 2.23$ kJ $mol^{-1}$ and $\sigma_{Ti} = 1.31$ Å, so as to approximately reproduce the Ti-O peak of the measured x-ray correlation function. L-J well depths and radii follow from the Lorentz-Berthelot mixing rules: $\varepsilon_{ij} = (\varepsilon_i\varepsilon_j)^{1/2}$ and $\sigma_{ij} = (\sigma_i + \sigma_j)/2$. Once equilibrated using the reference potentials, the empirical potential was permitted to become finite, and iteratively modified in order to achieve agreement with the measured x-ray structure factor.

### *D. Molecular Dynamics*

Classical molecular dynamics (MD) simulations were performed using the DLPOLY [43] code. Many interatomic potential parameterizations for titanium-oxygen systems exist in the literature, and we test here only the most recent or relevant. The only published simulations of liquid $TiO_2$ were made by Hoang [44,45], using the potentials of Matsui and Akaogi (MA) [46], which were those recommended after a review, by Collins *et al*. [47], of the existing potentials at the time (1996). We also assess the more recent potentials of Pedone *et al*. [48] (Pedone hereafter) and the rigid ion potentials of Teter [49], the latter of which are unpublished, but have been used extensively in the literature, particularly for the simulation of silicate glasses [49,50] and melts [51,52] (often with minor modifications). Both the MA and Teter pair potentials can be recast in the form

$$U_{ij}(r) = A_{ij}\exp[B_{ij}(\sigma_{ij} - r)] - \frac{C_{ij}}{r^6} - \frac{D_{ij}}{r^8} + f^2e^2\frac{q_iq_j}{4\pi\varepsilon_0 r}, \qquad (5)$$

where $q_i$ are formal ionic charges in units of the electron charge, *e*, $f \le 1$ is a charge scaling factor which is reduced from unity in order to simulate partial covalency, and $\varepsilon_0$ is the permittivity of free space. The parameter values used are given in Table I. The Pedone potentials are of the Morse form

$$U_{ij}(r) = E_{ij}\left[\left\{1-\exp\left(-k_{ij}(r-r_{ij})\right)\right\}^2 - 1\right] + f^2 e^2 \frac{q_i q_j}{4\pi\varepsilon_0 r}, \qquad (6)$$

and again the parameter values are given in Table I. Note that the full MA potentials include non-zero dispersion and repulsion terms between Ti-Ti pairs, however, we found that neglecting these terms made negligible difference to the resulting structure and so, as for the other models, Ti-Ti pairs interacted only via the repulsive Coulomb term. We also tested the potentials of Le Roux and Glasser [53], but these were rejected early on, on account of the resulting first Ti-O peak in $g_{\mathrm{TiO}}(r)$ being much too sharp, as compared to the diffraction data (and to the other MD models). Starting configurations of 4800 atoms were obtained by Monte Carlo simulation using the L-J plus Coulomb potentials introduced in the EPSR section above, with a fixed density of 3.210 g cm$^{-3}$. MD simulations were conducted either in the canonical (*NVT*) or the isothermal-isobaric (*NPT*) ensemble, using a Hoover-Nosé thermostat or thermostat-barostat, typically at $T = 2243$ K and $P = 1$ atm. A timestep of 1.0 fs was selected, with the first 1000 MD steps used for equilibration, and particle trajectories typically integrated over a further 49000 steps. The MA, Teter and Pedone potentials were all found to result in very low system densities in the *NPT* ensemble, as shown in Table I, with the Teter potentials resulting in the closest density to the expected 3.210 g cm$^{-3}$. In order to obtain the correct system density, the Teter potentials were softened by adding small attractive $-D_{ij}/r^8$ terms, and increasing the $A_{\mathrm{OO}}$ parameter, to which density is extremely sensitive, by 2%. These changes resulted in the 'Modified Teter' potentials, Table I. Although the modifications are by no means unique, they are small, result in negligible structural changes at a given density, and most importantly allow for the prediction of the system density as a function of $T$ and $P$. A new set of potentials, referred to as those of 'this work' (Table I) were derived (by heavy modification of the Teter potentials) in order to improve the agreement between simulated and measured x-ray structure factors, whilst also reproducing existing density data. The $A_{\mathrm{TiO}}$ parameter was initially greatly reduced, whilst also reducing $B_{\mathrm{TiO}}$ to maintain the Ti-O peak bond length at the position measured by x-ray diffraction. Non-Coulombic Ti-Ti interaction parameters were then introduced to broaden the Ti-Ti nearest neighbor peak and were adjusted iteratively, along with the density sensitive $A_{\mathrm{OO}}$ parameter. Repulsive short range $D_{ij}/r^8$ terms were added to remove the unphysical short range attraction which arises from the Buckingham potential terms. Densities derived from *NPT* simulations at different temperatures are shown in Fig. 1. In addition to MD simulations obtained from the identical (3.210 g cm$^{-3}$) starting configuration, with various target temperatures (grey squares, Fig. 1), a stepwise quench from 2198 K was also performed (grey circles, Fig. 1). In this case (again in the *NPT* ensemble) the temperature was lowered in 100 K steps down to 298 K, with 1000 equilibration and 24000 timesteps at each $T$ point, resulting in an average cooling rate of $4 \times 10^{12}$ K s$^{-1}$. In the case of the potentials of this work (see Table I), a starting temperature of 2798 K and 1500 atoms were used for an otherwise identical stepwise quench (blue diamonds, Fig. 1).

## IV. Results

The measured liquid structure factor is shown in Fig. 2a, and is compared to that for the powdered recovered material. Fig. 2b shows the higher resolution powder diffraction pattern obtained on the room temperature material, which closely matches the expected pattern for Rutile $TiO_2$. This is consistent with the zero mass loss measured, within uncertainty, and the < 1% oxygen deficiency thus inferred. The inset (Fig. 2b) reveals the presence of a very small phase impurity which could not be indexed according to any of the known $TiO_2$ polymorphs, nor the substoichiometric Magnéli phases, or indeed any known compound within the Ti-O phase diagram. It is possible that the unmatched Bragg peaks belong to a $Ti_nO_{2n-1}$ Magnéli phase with $n > 9$, or to an unknown modification of $TiO_2$. The powder pattern of the starting material (Rutile with Anatase impurity, Fig. 2b) serves to illustrate the peak broadening evident in the recovered material, arising from rapid solidification and resultant small crystallite sizes, although it is possible that the shoulders on the Rutile (110) peak at $d$ = 3.25 Å arise due to additional peaks from the unidentified phase impurity.

The short range structure, as evidenced by the $T(r)$ in Fig. 3a, differs significantly between crystalline Rutile, and the $TiO_2$ melt. Most markedly the first peak, arising due to Ti-O interatomic separations, shifts to shorter distance and reduces in area, both features indicative of a reduced Ti-O coordination number in the melt. Suitable integration of the function $r.T(r)$, Fourier transformed from the modified S(Q) – 1, with the Ti-O weighting ($W_{\mathrm{TiO}}(Q)$) divided out, yields a Ti-O coordination number of 5.0(2), with the peak (modal) bond-length 1.881(5) Å. The integration limits were 1.42 to 2.44 Å, the latter being the position of the first minimum to higher $r$ after the peak. Note however that $T(r)$ does not fall to zero at this minimum, there being a large overlap with other (O-O, Ti-Ti) correlations, and therefore the minimum in $T(r)$ may not correspond to a minimum in the partial $t_{\mathrm{TiO}}(r)$, resulting in an uncertainty which is difficult to quantify from x-ray diffraction alone. As such it is necessary to generate models in order to aid interpretation of the data. Nonetheless, the average value of $n_{\mathrm{TiO}}$ = 5.0(2) represents an *upper bound* (for the given cutoff), and so the reduction of $n_{\mathrm{TiO}}$ in the melt, below the value of 6 in all known crystalline phases of $TiO_2$ is clear. This is supported by the reduced peak position of 1.881(5) Å (*cf*. 1.962(5) Å in Rutile, Table II) which is consistent with 5-fold units, [$TiO_5$], based on bond-valence, assuming five equivalent bonds (of 1.898 Å), and neglecting any thermal expansion of the bonds at high temperature. Fig. 3b demonstrates the efficacy of the high energy x-ray diffraction technique employed by comparing $T(r)$ measured for the recovered Rutile material to that simulated based on the long-range averaged structure (known unit cell). Thermal broadenings (which do not follow from the crystallographic thermal parameters due to possible correlated motion at short-range) were adjusted to be similar to the measurements ($\langle u^2_{\mathrm{TiO}}\rangle^{1/2}$ = 0.100 Å, $\langle u^2_{\mathrm{OO}}\rangle^{1/2}$ = 0.072 Å, $\langle u^2_{\mathrm{TiTi}}\rangle^{1/2}$ = 0.116 Å). Direct peak fitting to the Ti-O peak yielded the position $r_{\mathrm{TiO}}$ = 1.962(5) Å and $n_{\mathrm{TiO}}$ = 5.7(2), the latter being 4% smaller than the expected value, and a measure of the overall uncertainty of coordination numbers determined from both solid and liquid phase datasets. Table II summarizes the pertinent values obtained.

A key finding of the molecular dynamics modelling study was that, in the *NPT* ensemble, all of the preexisting potential models tested would drive the system towards a density much lower than expected from the experimental measurements [39] (Table I). As discussed above, the potentials of this work and the modified Teter potentials were adjusted in order to give the expected density at 2250 K. Figure 1 compares the densities obtained with these two sets of potentials over a wide temperature range, where they show excellent agreement with experimental data, including that for the densest (lowest porosity [17]) amorphous $TiO_2$ films at room temperature. Fig. 4 compares the experimentally weighted model interference functions directly with the experimental data. By construction, the EPSR model gives an excellent fit, while all of the preexisting MD models predict sharper features in the structure factor than those observed in the measured data. It was for this reason that we chose to derive a new set of potentials, in order to better simulate the measured liquid structure factor. We note that the potentials derived by EPSR may also be used for MD, but that they take a more cumbersome analytical form (the empirical terms comprise a sum of Poisson curves), or may be used in numerical form. Quantitative comparison of the models is made with reference to the real-space functions shown in Fig. 5 and using the quality-of-fit parameter [54]

$$R_\chi(r_{k,\max}) = \left( \frac{\sum_{k=1}^{k,\max} \left[ T_{\exp}(r_k) - T_{\mathrm{mod}}(r_k) \right]^2}{\sum_{k=1}^{k,\max} T_{\exp}^2(r_k)} \right)^{1/2} , \tag{7}$$

where subscripts exp and mod denote experimental and modelled functions respectively. The $R\chi$ calculated for each model ($1.2 \leq r_k \leq 10.0$ Å) are recorded in Table II, showing that those of this work are the best, by this measure. The dependence of $R\chi$ on the maximum cutoff distance, $r_{k,max}$, is shown in Fig. 6. Both the Matsui & Akaogi [46] and the Pedone *et al*. [48] potentials give rise to total x-ray $T(r)$ functions (Fig. 5) which are over structured at high $r$, while the like and unlike pair functions, $t_{ij}(r)$, derived using the modified Teter and potentials of this work are in anti-phase and of sufficient amplitude, so as to reproduce the rather flat and featureless $T(r)$ measured experimentally for $r > 5$ Å. Furthermore, Table II shows that the Matsui & Akaogi [46] and Pedone *et al*. [48] potentials respectively over- and underestimate the peak Ti-O bond length. For each model, coordination numbers, $n_{\mathrm{TiO}}$, obtained from the Ti-O partial radial distribution functions, $4\pi\rho c_O r^2 g_{\mathrm{TiO}}(r)$, fall slightly below the value 5.0(2) determined directly from the diffraction data (cutoff 2.44 Å, Table II). According to most of the models, this is partly due to the inclusion of intensity from the O-O partial in the experimentally determined value.

## V. Discussion

### A. Densities of liquid, amorphous and crystalline $TiO_2$

Extrapolating the thermal expansion trend for Rutile measured by Henderson *et al*. [55], the density at the melting point (2135 K) is 4.04 gcm$^{-3}$, while interpolating for the liquid trend from Dingwell [39], the density is 3.24 gcm$^{-3}$, giving a large density drop of 20% on melting (or 25% increase on crystallization, Fig. 1a). This is of very similar magnitude to that observed for the Corundum→liquid $Al_2O_3$ [28] and Quartz→liquid $SiO_2$ [56] transitions. The $SiO_2$ melting transition is not accompanied by a change in coordination number [56,57], but the $Al_2O_3$ melting is (where $n_{\mathrm{AlO}}$ drops from 6.0 to 4.4 [28]). This has been attributed by Skinner *et al*. [26] essentially to the higher field strength of $Si^{4+}$. Our finding that $n_{\mathrm{TiO}}$ drops on melting is consistent with this picture based on the similar field strengths of $Ti^{4+}$ and $Al^{3+}$.

The structure of liquid $TiO_2$ has previously been simulated by Hoang [44,45] using MD and the potentials of Matsui & Akaogi (MA) [46]. These were however conducted at *fixed* densities, independent of temperature, with the lowest liquid density used, 3.80 g cm$^{-3}$, corresponding to that of dense amorphous $TiO_2$ films [17], and much higher than the measured values [39] for the liquid. The structure and properties thus derived are therefore more pertinent to the *high pressure* liquid, where both density and coordination numbers would be higher. With the slight modifications made in the present work to the Teter potentials, we were able to obtain the expected density (based on [39]) at 2250 K, and using these potentials, we estimate that the high liquid density of 3.80 g cm$^{-3}$ used by Hoang [44,45] corresponds to a pressure of 4.8 GPa (note that the *model* pressure using the MA potentials would be much higher: 65 GPa at 2250 K and 3.21 g cm$^{-3}$). Both the modified Teter potentials, and those of this work, allow for the prediction of the density $\rho(T)$ over a wide range of temperatures, over much of the experimentally stable liquid region, and through supercooling to form glassy $TiO_2$. Both the experimentally determined thermal expansion of the liquid [39], and the density of the amorphous phase are reproduced by our models, Fig. 1. The experimental densities of amorphous $TiO_2$ films vary greatly [17], although those with lower density typically have higher porosity, and we naturally expect dense, pore free, models to be close to the upper end of the experimental values, as found (Fig. 1a). The slightly lower density of our models compared to the upper bound of experimental amorphous $TiO_2$ densities may be a result of the rapid quenching necessary in MD simulations, which is supported by the comparison between models cooled at 4 x 10$^{12}$ K s$^{-1}$ (blue diamond, Fig. 1a, $T$ = 298 K) and at 100 x 10$^{12}$ K s$^{-1}$ (open orange square, Fig. 1a, $T$ = 298 K), the larger rate resulting in a 3% decrease in density. First principles MD models of amorphous $TiO_2$ have been obtained [58] with densities of 3.56 to 3.59 g cm$^{-3}$; essentially the same as that found here (3.57(1) g cm$^{-3}$).

If fixed density simulations are to be performed, then the importance of the choice of density parameter, when modelling any condensed phase, cannot be underestimated. This is clear, for example, from the strong dependence of $n_{\mathrm{TiO}}$ on density in models of liquid and amorphous $TiO_2$ [44,45,59,60], and from the following discussion sections V. B – V. D. The advantage of models capable of predicting density, such as those used here, is therefore significant.

### B. *Thermal Expansion*

The volume thermal expansion coefficients, $\alpha_V$, can be calculated from the variation in density with temperature, $\rho(T)$, using

$$\alpha_V = \left( \frac{\rho(T_R)}{\rho(T)} - 1 \right) \frac{1}{\Delta T} = \frac{1}{V(T_R)} \left( \frac{\Delta V}{\Delta T} \right), \tag{8}$$

where Δ denotes a difference in density, $\Delta\rho = \rho(T_R) - \rho(T)$, volume, $\Delta V = V(T) - V(T_R)$, or temperature, $\Delta T = T - T_R$, and $T_R$ = 298 K is a chosen reference temperature. Table III records the modelled $\alpha_V$ over the linear expansion regions, where it can be seen that the modelled amorphous phase $TiO_2$ shows very similar, though slightly larger, expansion compared to Rutile $TiO_2$ [55]. For the liquid phase the modelled $\alpha_V$ are much larger than for the solid phases, and smaller than that derived from Dingwell's measurements [39] on the melt, by 8% in the case of the improved potentials of this work, and 21% for the Teter potentials. The origin of the discrepancies is not clear, but it should be noted that the experimental value is based on only two density measurements plus one extrapolated point from $CaSiO_3$-$TiO_2$ pseudobinary melts, and covers a smaller temperature range (Table III) than the modelled values. The large $\alpha_V$ of the melt is due, in part, to temperature dependent structural changes (discussed in section V. D.).

It is remarkable that Henderson *et al*. [55] have shown that the thermal expansion of the two longer, axial, Ti-O bonds within the $[TiO_6]$ octahedron of Rutile $TiO_2$ is more than 7 times larger than that of the four shorter, equatorial bonds. This can be considered as a precursory effect to the reduction of the average $n_{TiO}$ upon melting, from 6 to about 5 in the melt.

### C. *Local Structure of Liquid TiO₂*

The $t_{ij}(r)$ of the EPSR, MD (this work) and three literature MD models (Fig. 5) show some significant differences and similarities. For example, the $t_{OO}(r)$ are mostly very similar, except for that of the MA MD model, which is much sharper. Indeed, while, of the three *literature* MD models, the first (Ti-O) peak of the MA model reproduces the experimental data most closely (Figs. 5 & 6), at higher $r$ the $t_{TiO}(r)$ is the most different from the other models, showing a pronounced shoulder of the 2nd Ti-O peak at about 4.0 Å. The oversharpness of the $t_{ij}(r)$ peaks in the liquid $TiO_2$ models obtained using the literature potentials is related to their high melting points in the Rutile phase. These were all found to be > 2843 K, and much greater in the case of the MA potentials, and hence much greater than the experimental melting point of 2135 K. In deriving the potentials of this work (Table I), and obtaining an improved simulation of the melt structure, the model Rutile melting point was incidentally also reduced, toward the experimental value, but remaining higher at about 2470(80) K.

The structural characteristics of both the EPSR and best MD model were looked into in more detail. The average coordination numbers $n_{TiO}$ and $n_{OTi} = (1/2)n_{TiO}$ are broken down into their distributions in Fig. 7a. The majority species are 5-fold $[TiO_5]$ polyhedra, having around 50% abundance, with the remaining Ti being either 4-fold or 6-fold, with slightly more of the latter (cutoff dependent, Fig.7b). Given the average $n_{TiO}$ of about 5 (Table II), the average $n_{OTi}$ is about 2.5, with about half of the oxygen atoms bonded to two Ti, in 'bridging-oxygen like' environments, and the other half to three Ti, in 'crystalline $TiO_2$ like' local environments. This implies a large degree of corner-sharing, as well as edge-sharing, between $[TiO_m]$ polyhedra. This fact is also manifest in the asymmetry of the first peak in the $t_{TiTi}(r)$, which, in the amorphous phase at room temperature, is resolved into two separate Ti-Ti peaks in our model. Such splitting of the Ti-Ti peak has been observed previously [20,45,58] in amorphous $TiO_2$. Fig. 7c shows bond angle distributions (BADs) for the EPSR and modified Teter MD models, where again there is broad qualitative agreement, and some quantitative differences. The partial bond angle distributions (not shown) reveal that the various polyhedra are not overly distorted, for example, the 4-fold $[TiO_4]$ are tetrahedral, with mean O-Ti-O angle of 109.1°.

### D. *Temperature Dependence of the Liquid Structure*

The temperature dependence of the average coordination numbers derived using the new MD potentials are shown in Fig. 8. It is clear that the liquid structure is in fact weakly temperature dependent, the average coordination numbers displaying a gradual decline with increasing temperature. A fit to the liquid data up to 2798 K yields a temperature coefficient of $-3.0(1) \times 10^{-4}$ $K^{-1}$ for $n_{TiO}$ (dashed line in Fig. 8, full precision trend given in Fig. 8 caption, see also Table III), equivalent to -5.8(2) x $10^{-3}$ % $K^{-1}$ compared to the values at the melting point, for both Ti-O and O-Ti coordination numbers. Hence over the whole range of liquid stability, which is of order $10^3$ K, the $n_{ij}$ are expected to change by only about 6%.

Melt fragility measures the degree of deviation from Arrhenian behavior of the liquid viscosity, and has been directly related to the temperature dependence of the number of degrees of freedom per atom [61-63]. Hence the observed temperature dependence of the coordination numbers is expected to contribute to an increased liquid fragility, as well as to the large thermal expansion coefficient (see Table III and Fig. 1). The authors are not aware of any viscosity measurements on pure $TiO_2$ melts.

Below the melting point, in the supercooled liquid region, the points in Fig. 8 deviate from linearity, and from the extrapolated trend shown by the dashed line. This is related to the fact that the system densities (Fig. 1) also deviate from a smooth trend in this region, and the inset to Fig. 8 shows the strong correlation between density and $n_{\mathrm{TiO}}$. Taking into account the temperature dependence of the position of the first minimum in $g_{\mathrm{TiO}}(r)$ to define the coordination numbers (light squares, Fig. 8) does not remove the deviation. We attribute the deviations in density and the $n_{ij}$ to the sensitivity of the simulations to finite size and timescale effects in the high viscosity, supercooled liquid region, as discussed by Micoulaut *et al*. [64]. Using the variable cutoff trend (Fig. 8), the difference between $n_{\mathrm{TiO}}$ for the liquid at the melting point and amorphous $TiO_2$ at room temperature is 0.23, or 4.3%, which is smaller than the 6.0% indicated by the trend obtained using a fixed cut-off of 2.75 Å to define $n_{\mathrm{TiO}}$.

The strong correlation between liquid density and structure is characterized by the gradient $d\rho/dn_{\mathrm{TiO}}$ = 0.0183(3) atoms $Å^{-3}$ (see Fig. 8 inset), derived by combining the data of Fig. 1 and Fig. 8. This value is in agreement with that predicted by fixed density *ab initio* MD simulations of amorphous $TiO_2$ (0.0173(5) $Å^{-3}$ [59]).

We have determined the hypothetical glass transition temperature from our molecular dynamics models using the discontinuity in the model potential energy, after Micoulaut et al. [64], Table III. Using the modified Teter potentials, a value comparable to the $T_g$ determined by Hoang [44,45] using MD with the MA potentials, at higher (fixed) densities of 3.80 g $cm^{-3}$ to 4.20 g $cm^{-3}$, is obtained, whist a lower value is obtained using the potentials of this work. Due to the lack of an experimentally observed glass transition, it is difficult to comment on the relative merits of each prediction. During experiments we rarely observed supercooling of the melt owing to the existence of a top-to-bottom temperature gradient and the presence of small crystallites in the bottom of the sample, well away from the laser heated liquid upper region probed by x-ray diffraction and pyrometry. This compromise was accepted because upon full melting of the sample, it would tend to destabilize and adhere to the nozzle such that the experiment had to be terminated. On one occasion during later testing, a stable melt was obtained, and supercooling was observed down to the onset of recalescence at 1580 K. Hence it is possible that the theoretical glass transition temperatures are testable if the cooling rate can be increased above the observed 177(2) K $s^{-1}$ (at 1580 K).

### E. *Comparison to High Pressure Liquid $SiO_2$*

It is well known that crystalline $TiO_2$ represents an analogue to $SiO_2$ at higher pressures [21]. Indeed, as pressure is applied to Quartz $SiO_2$, it transforms first to Coesite and then to Stishovite, which is stable above about 8.7 GPa. Stishovite has the Rutile structure, which is the most common naturally occurring structure for $TiO_2$.

Given the above, we investigate the extension of this analogy to the liquid state. Liquid $TiO_2$ at ambient pressure has an average $n_{TiO}$ close to 5, while liquid silica has $n_{SiO} = 4$ [56,57]. However, as pressure is increased, it has been shown both experimentally for $SiO_2$ glass [65,66], and computationally for $SiO_2$ liquid [67,68], that the average Si-O coordination increases. We can therefore estimate the pressure of the analogous $SiO_2$ melt as that at which silicon is 5-fold coordinated to oxygen. In the glass this is at about 27 GPa [65,66], and is comparable to existing *ab initio* calculations for the melt at 3500 K and 27 GPa [67] ($n_{SiO} = 4.76$) or 3000 K and 20 GPa [68] ($n_{SiO} = 4.68$). Such pressures for the liquid correspond to "molten Stishovite", being well above the equilibrium phase fields for Quartz and Coesite. Calculated coordination number distributions for molten silica are compared to those for $TiO_2$ in Fig. 7a, showing some similarity, although the comparison is rather qualitative given the mismatches in average coordination number (owing to the availability of liquid silica data only at discreet pressure values [67,68]). Fig. 9 compares the measured x-ray structure factors for ambient pressure liquid titania and silica glass at 27 GPa. Despite small differences in x-ray scattering weighting factors, and the large temperature difference, the two functions show considerable similarity, plotted using the dimensionless quantity $r_1Q$, with $r_1$ the nearest neighbor bond length taken from the measured $T(r)$.

We note that $GeO_2$ represents a further analogue to the $TiO_2$ and $SiO_2$ melts, with germania *glass* having an average Ge-O coordination number of five at intermediate pressure, determined by various authors to be about 14.5 GPa [69] (neutron diffraction), 10.5 GPa [70] (x-ray diffraction) or 11 GPa [64] (classical MD). Indeed, it is likely that the melts of $HfO_2 \rightarrow ZrO_2 \rightarrow TiO_2 \rightarrow GeO_2 \rightarrow SiO_2$ form a series of structural analogues at increasing pressures, from left to right, and potentially with other oxides based on tetravalent cations such as Sn, Pb, U, Th etc., where the various pressures for isomorphic liquid pairs remain to be determined. For example, molten $ZrO_2$ at ambient pressure has $n_{ZrO} = 6.1(4)$ [26], a coordination number which would be obtained in molten $TiO_2$ only at elevated pressures. This is comparable to the crystalline state where Rutile $TiO_2$ transforms at 12 GPa [71] into a phase isomorphous with ambient Baddeleyite $ZrO_2$, with 7-fold cations.

### F. *$TiO_2$ Polymorphs with Low Ti-O Coordination*

Given the stable existence of 5-fold, as well as 4-fold, coordinated titanium in liquid $TiO_2$, as well as in several complex crystalline and glassy titanates, it is natural to speculate on the existence of metastable crystalline $TiO_2$ polymorphs containing Ti with coordination number less than six, in contrast to the majority of known ambient pressure polymorphs [21,72]. In fact, recent refinements of diffraction data, and density functional theoretic calculations [23] have been used to show that the $TiO_2$(B) polymorph can be considered as having $n_{TiO} = 5.5$, being composed of equal numbers of 6-fold and 5-fold Ti polyhedra with the latter having one additional long, very weak bond. Moreover, monolayer nanosheets of this polymorph can be composed entirely of 5-fold Ti [73-75].

It is interesting to note that Lacks and Gordon [76] have shown, using a polarization-included electron-gas model, that $TiO_2$ placed in the Quartz structure (4-fold [$TiO_4$] tetrahedra) at ambient pressure is metastable, and relaxes toward a higher pressure version of the Quartz $SiO_2$ structure, with reduced X-O-X bond angles. Furthermore, the authors [76] found Quartz $TiO_2$ to be *stable*, relative to the Rutile form, at a *negative* pressure of -5 GPa. Hypothetical Coesite $TiO_2$ (also built from 4-fold [$TiO_4$] tetrahedra) could therefore be expected to be stable at more modest negative pressures, given that it is the silica polymorph stable at pressures intermediate between the Quartz and Stishovite phase fields, and also to be metastable at ambient pressure (although no such phase is observed for $GeO_2$). Very recently, $TiO_2$ in the Tridymite structure (a high *T* polymorphic form of $SiO_2$, also containing tetrahedral cations) has also been shown to be metastable at ambient pressure [77]. But what of hypothetical $TiO_2$ structures built from 5-fold [$TiO_5$] polyhedra, or with mixed Ti coordination states? Such structures should also be expected to be metastable with respect to Rutile, but even closer in free-energy and density to the aforementioned, compared to the 4-fold structures. $MO_2$ structures based entirely on [$MO_5$] polyhedra are very rare. We are aware only of a vanadium dioxide polymorph, $VO_2$(C), which is a layered compound composed of sheets of [$VO_5$] square pyramids [78,79], although full crystallographic data has not been published, possibly due to nonstoichiometry and the retention of Li or $H_2O$ from the synthesis route.

There are other reasons for considering the existence of energetically competitive $TiO_2$ polymorphs based on Ti coordination polyhedra with fewer than 6 ligands. The semi-empirical model of ideal associated solutions (IAS) [80] is used to predict the chemical structure of liquids and glasses based on the law of mass action and the free energies of the stoichiometric compounds within a given phase diagram (e.g. pseudo-binary $MO_x$-$JO_y$), as functions of *T*, *P* and composition. The IAS model has been applied successfully to model various properties of glasses at room temperature [80], as well as to predict variation of coordination numbers in oxide melts as a function of *T* [81,82]. Typically however, only high-temperature polymorphs, of congruently melting stoichiometries are considered. This means that for end-member oxides, such as $TiO_2$, no change in coordination number between high temperature stable crystalline phase (Rutile) and melt is predicted, in contrast to the experimental observations of the present work. The standard IAS model is therefore not applicable to many single oxide systems, such as $TiO_2$ and $Al_2O_3$, as well as to $TiO_2$ or $Al_2O_3$ rich multi-component systems, to name but a few examples where differences between crystal and melt (or glass) cation-oxygen coordination number have been observed and recently reviewed [26].

In a binary oxide melt, the standard IAS model can be used to predict the fractions of various stoichiometric groupings, which exist locally within the liquid. Thus the model implicitly relies upon local compositional fluctuations which are expected to occur in the melt. In a single oxide liquid, no such local compositional fluctuations are expected, but local density fluctuations may still occur, and these are associated not with other possible stoichiometries, but with other possible polymorphs which are sampled locally as regions of the melt explore the underlying energy landscape. This is qualitatively similar to the concept of polymorphoids expounded by Minaev *et al*. [83], and related phenomenology is important in the concepts of polyamorphism and liquid-liquid phase transitions [84].

Therefore, considering a modified IAS model, where not only high-temperature stable, but all energetically competitive polymorphs are included, the low cation-oxygen coordination observed in liquid $TiO_2$ in this work, and for various other oxide melts and glasses [26], implies, at least in the case of single oxide systems, the existence of energetically competitive crystalline polymorphs, also with cation-oxygen coordination numbers lower than for the high-temperature stable phase. Comparison can be made to the $Al_2O_3$ system, in which molten alumina has $n_{\mathrm{AlO}} = 4.4$ [28], the stable crystal polymorph, Corundum, has $n_{\mathrm{AlO}} = 6.0$, but several metastable polymorphs exist (such as γ-$Al_2O_3$) with mixed tetrahedral-octahedral coordination [30] and, on average, $4 < n_{\mathrm{AlO}} < 6$.

We suggest that experimental and theoretical searches for 'low-coordinated' materials, such as $TiO_2$ based on 5-fold Ti-O polyhedra, may prove fruitful. These are expected to have lower densities than the more highly coordinated structures, such as the 6-fold Rutile phase, but higher or similar densities to the microporous Ramsdellite (R) and $TiO_2$(B) and mesoporous Hollandite (H) $TiO_2$ polymorphs (see Fig. 1a), the latter of which is even less dense than amorphous $TiO_2$, Fig. 1a. Evolutionary crystal structure prediction has been applied to the $TiO_2$ system previously [85], but in that case the search was intentionally biased towards materials with high hardness, which turned out to be composed of 7-fold or 6-fold Ti, similar to the known high pressure phases of $TiO_2$.

## VI. Conclusions

High energy x-ray diffraction measurements on molten $TiO_2$ have revealed an average Ti-O coordination number close to 5.0(2). MD and EPSR models that are in the best agreement with the diffraction data suggest that the structure is based on lower coordination polyhedra (mainly 5-fold [$TiO_5$]) than the vast majority of the known crystalline polymorphs, which contain only octahedral titanium at ambient pressure. This finding is in qualitative accord with a recently observed trend [26] for oxide melts, toward lower-than-crystal coordination numbers, with the effect being larger for lower field strength cations.

We have obtained classical molecular dynamics potentials which reproduce the structure of molten $TiO_2$ better than any other published potentials. In addition, our potentials are able to reproduce the liquid and amorphous state densities and thermal expansions of $TiO_2$, in agreement with literature data. This is of critical importance given the strong correlation between density and structural parameters such as $n_{\mathrm{TiO}}$. An associated prediction is a weakly temperature dependent liquid structure, which contributes to the large thermal expansion of the melt.

We argue on the basis of our result that metastable polymorphs of $TiO_2$, based on lower-than-octahedral Ti-O polyhedra, may yet be obtained, either experimentally and/or computationally. This is somewhat in analogy to the known polymorphism and liquid structure of alumina.

Liquid titania represents a structural analogue to molten silica at higher pressure, estimated to be in the region of 27 GPa. As such, the study of more complex titanate melts may well open a window on the structure and properties of geologically relevant silicate melts at high pressure.

## Acknowledgements

Use of the Advanced Photon Source, an Office of Science User Facility operated for the U.S. Department of Energy (DOE) Office of Science by Argonne National Laboratory, was supported by the U.S. DOE under Contract No. DE-AC02-06CH11357. OLGA, JKRW, AT and CJB were supported by U.S. DOE grant No. DE-SC0007564 and LBS by U.S. DOE BES DE-FG02-09ER46650. We thank the anonymous referees for their constructive comments which led to numerous improvements to the manuscript.

## References

[1] A. Fujishima, T. N. Rao, and D. A. Tryk, J. Photochem. Photobiol., C **1**, 1 (2000).
[2] U. I. Gaya and A. H. Abdullah, J. Photochem. Photobiol., C **9**, 1 (2008).
[3] M. Cologna, J. S. C. Francis, and R. Raj, J. Eur. Ceram. Soc. **31**, 2827 (2011).
[4] J. Narayan, Scripta Mater. **69**, 107 (2013).
[5] R. Raj, J. Eur. Ceram. Soc. **32**, 2293 (2012).
[6] S. John Paul, J. J. Yang, M. Ruth, S. Andreas, M.-R. Gilberto, R. S. Duncan, and R. S. Williams, Nanotechnology **20**, 485701 (2009).
[7] D. B. Strukov, G. S. Snider, D. R. Stewart, and R. S. Williams, Nature **453**, 80 (2008).
[8] D.-H. Kwon *et al.*, Nat. Nanotechnol. **5**, 148 (2010).
[9] J. J. Yang, D. B. Strukov, and D. R. Stewart, Nat. Nanotechnol. **8**, 13 (2013).
[10] J. M. Knaup, J. Marx, and T. Frauenheim, Phys. Status Solidi RRL **8**, 549 (2014).
[11] G. Handfield and G. G. Charette, Can. Metall. Quart. **10**, 235 (1971).
[12] D. R. Sadoway, J. Mater. Res. **10**, 487 (1995).
[13] N. A. Fried, K. G. Rhoads, and D. R. Sadoway, Electrochim. Acta **46**, 3351 (2001).
[14] A. Masuno, H. Inoue, J. Yu, and Y. Arai, J. Appl. Phys. **108**, 063520 (2010).
[15] S. D. Stookey, Ind. Eng. Chem. **51**, 805 (1959).
[16] G. Beall, Int. J. Appl. Glass. Sci. **5**, 93 (2014).
[17] D. Mergel, D. Buschendorf, S. Eggert, R. Grammes, and B. Samset, Thin Solid Films **371**, 218 (2000).
[18] J. Yu *et al.*, Chem. Mater. **21**, 259 (2009).
[19] L. Cormier, P. H. Gaskell, G. Calas, and A. K. Soper, Phys. Rev. B **58**, 11322 (1998).
[20] V. Petkov, G. Holzhüter, U. Tröge, T. Gerber, and B. Himmel, J. Non-Cryst. Solids **231**, 17 (1998).
[21] Z. Fu, Y. Liang, S. Wang, and Z. Zhong, Phys. Status Solidi B **250**, 2206 (2013).
[22] Y. Le Page and P. Strobel, J. Solid State Chem. **44**, 273 (1982).
[23] M. B. Yahia, F. Lemoigno, T. Beuvier, J.-S. Filhol, M. Richard-Plouet, L. Brohan, and M.-L. Doublet, J. Chem. Phys. **130**, 204501 (2009).
[24] J. Gunter and G. Jameson, Acta Crystallogr. C **40**, 207 (1984).
[25] K. K. Wu and I. Brown, Acta Crystallogr. B **29**, 2009 (1973).
[26] L. B. Skinner, C. J. Benmore, J. K. R. Weber, J. Du, J. Neuefeind, S. K. Tumber, and J. B. Parise, Phys. Rev. Lett. **112**, 157801 (2014).
[27] S. Ansell, S. Krishnan, J. K. R. Weber, J. J. Felten, P. C. Nordine, M. A. Beno, D. L. Price, and M.-L. Saboungi, Phys. Rev. Lett. **78**, 464 (1997).
[28] L. B. Skinner *et al.*, Phys. Rev. B **87**, 024201 (2013).
[29] C. Landron, L. Hennet, T. E. Jenkins, G. N. Greaves, J. P. Coutures, and A. K. Soper, Phys. Rev. Lett. **86**, 4839 (2001).
[30] I. Levin and D. Brandon, J. Am. Ceram. Soc. **81**, 1995 (1998).
[31] D. A. Keen, J. Appl. Cryst. **34**, 172 (2001).
[32] E. Lorch, J. Phys. C **2**, 229 (1969).

[33] U. Rütt, M. A. Beno, J. Strempfer, G. Jennings, C. Kurtz, and P. A. Montano, Nucl. Instrum. Meth. A **467–468**, 1026 (2001).

[34] J. K. R. Weber, S. Krishnan, C. D. Anderson, and P. C. Nordine, J. Am. Ceram. Soc. **78**, 583 (1995).

[35] L. B. Skinner, C. J. Benmore, and J. B. Parise, Nucl. Instrum. Meth. A **662**, 61 (2012).

[36] J. K. R. Weber, J. J. Felten, and P. C. Nordine, Rev. Sci. Instrum. **67**, 522 (1996).

[37] X. Qiu, J. W. Thompson, and S. J. L. Billinge, J. Appl. Cryst. **37**, 678 (2004).

[38] A. K. Soper and E. R. Barney, J. Appl. Cryst. **44**, 714 (2011).

[39] D. B. Dingwell, J. Am. Ceram. Soc. **74**, 2718 (1991).

[40] D. B. Dingwell, Geochim. Cosmochim. Ac. **56**, 3403 (1992).

[41] A. K. Soper, Phys. Rev. B **72**, 104204 (2005).

[42] O. L. G. Alderman, A. C. Hannon, D. Holland, S. Feller, G. Lehr, A. J. Vitale, U. Hoppe, M. Von Zimmermann, and A. Watenphul, Phys. Chem. Chem. Phys. **15**, 8506 (2013).

[43] W. Smith and T. R. Forester, J. Mol. Graphics **14**, 136 (1996).

[44] V. V. Hoang, J. Phys.: Condens. Matter **19**, 416109 (2007).

[45] V. V. Hoang, Phys. Status Solidi B **244**, 1280 (2007).

[46] M. Matsui and M. Akaogi, Mol. Sim. **6**, 239 (1991).

[47] D. R. Collins, W. Smith, N. M. Harrison, and T. R. Forester, J. Mater. Chem. **6**, 1385 (1996).

[48] A. Pedone, G. Malavasi, M. C. Menziani, A. N. Cormack, and U. Segre, J. Phys. Chem. B **110**, 11780 (2006).

[49] A. N. Cormack, J. Du, and T. R. Zeitler, Phys. Chem. Chem. Phys. **4**, 3193 (2002).

[50] J. Du and A. N. Cormack, J. Non-Cryst. Solids **349**, 66 (2004).

[51] C. J. Benmore, J. K. R. Weber, M. C. Wilding, J. Du, and J. B. Parise, Phys. Rev. B **82**, 224202 (2010).

[52] L. B. Skinner, C. J. Benmore, J. K. R. Weber, S. Tumber, L. Lazareva, J. Neuefeind, L. Santodonato, J. Du, and J. B. Parise, J. Phys. Chem. B **116**, 13439 (2012).

[53] H. le Roux and L. Glasser, J. Mater. Chem. **7**, 843 (1997).

[54] A. C. Wright, in *Experimental Techniques of Glass Science*, edited by C. J. Simmons, and O. H. El-Bayoumi (The American Ceramic Society, Westerville, Ohio, 1993), pp. 205.

[55] C. Henderson, K. Knight, and A. Lennie, Open Mineralogy Journal **3**, 1 (2009).

[56] L. B. Skinner, C. J. Benmore, J. K. R. Weber, M. C. Wilding, S. K. Tumber, and J. B. Parise, Phys. Chem. Chem. Phys. **15**, 8566 (2013).

[57] Q. Mei, C. J. Benmore, and J. K. R. Weber, Phys. Rev. Lett. **98** (2007).

[58] B. Prasai, B. Cai, M. K. Underwood, J. P. Lewis, and D. Drabold, J. Mater. Sci. **47**, 7515 (2012).

[59] T. Köhler, M. Turowski, H. Ehlers, M. Landmann, D. Ristau, and T. Frauenheim, J. Phys. D: Appl. Phys. **46**, 325302 (2013).

[60] M. Landmann, T. Köhler, E. Rauls, T. Frauenheim, and W. G. Schmidt, J. Phys.: Condens. Matter **26**, 253201 (2014).

[61] G. G. Naumis, Phys. Rev. E **71**, 026114 (2005).

[62] J. C. Mauro, P. K. Gupta, and R. J. Loucks, J. Chem. Phys. **130**, 234503 (2009).

[63] P. K. Gupta and J. C. Mauro, J. Chem. Phys. **130**, 094503 (2009).

[64] M. Micoulaut, Y. Guissani, and B. Guillot, Phys. Rev. E **73**, 031504 (2006).

[65] T. Sato and N. Funamori, Phys. Rev. B **82**, 184102 (2010).

[66] C. J. Benmore, E. Soignard, S. A. Amin, M. Guthrie, S. D. Shastri, P. L. Lee, and J. L. Yarger, Phys. Rev. B **81**, 054105 (2010).

[67] A. Trave, P. Tangney, S. Scandolo, A. Pasquarello, and R. Car, Phys. Rev. Lett. **89**, 245504 (2002).

[68] B. B. Karki, D. Bhattarai, and L. Stixrude, Phys. Rev. B **76**, 104205 (2007).

[69] P. S. Salmon *et al.*, J. Phys.: Condens. Matter **24**, 415102 (2012).

[70] Q. Mei, S. Sinogeikin, G. Shen, S. Amin, C. J. Benmore, and K. Ding, Phys. Rev. B **81**, 174113 (2010).

[71] L. Gerward and J. Staun Olsen, J. Appl. Cryst. **30**, 259 (1997).

[72] V. Swamy, J. D. Gale, and L. Dubrovinsky, J. Phys. Chem. Solids **62**, 887 (2001).

[73] A. Vittadini, F. Sedona, S. Agnoli, L. Artiglia, M. Casarin, G. A. Rizzi, M. Sambi, and G. Granozzi, ChemPhysChem **11**, 1550 (2010).

[74] A. Vittadini, M. Casarin, and A. Selloni, Theor. Chem. Acc. **117**, 663 (2007).

[75] F. De Angelis, C. Di Valentin, S. Fantacci, A. Vittadini, and A. Selloni, Chem. Rev., Article ASAP DOI: 10.1021/cr500055q (2014).

[76] D. J. Lacks and R. G. Gordon, Phys. Rev. B **48**, 2889 (1993).

[77] T. Zhu and S.-P. Gao, J. Phys. Chem. C **118**, 11385 (2014).

[78] T. A. Chirayil, P. Y. Zavalij, and M. S. Whittingham, J. Electrochem. Soc. **143**, L193 (1996).

[79] D. Hagrman, J. Zubieta, C. J. Warren, L. M. Meyer, M. M. Treacy, and R. C. Haushalter, J. Solid State Chem. **138**, 178 (1998).

[80] B. A. Shakhmatkin, N. M. Vedishcheva, M. M. Shultz, and A. C. Wright, J. Non-Cryst. Solids **177**, 249 (1994).

[81] M. Liška, J. Macháček, P. Perichta, O. Gedeon, and J. Pilát, Ceram-Silikaty **52**, 61 (2008).

[82] N. M. Vedishcheva, B. A. Shakhmatkin, and A. C. Wright, Phys. Chem. Glasses **41**, 260 (2000).

[83] V. S. Minaev, S. P. Timoshenkov, and V. V. Kalugin, Phys. Status Solidi C **8**, 2701 (2011).

[84] P. F. Mcmillan, M. Wilson, M. C. Wilding, D. Daisenberger, M. Mezouar, and G. N. Greaves, J. Phys.: Condens. Matter **19**, 415101 (2007).

[85] A. O. Lyakhov and A. R. Oganov, Phys. Rev. B **84**, 092103 (2011).

[86] E. Meagher and G. A. Lager, Can. Mineral. **17**, 77 (1979).

[87] M. Horn, C. Schwerdtfeger, and E. Meagher, Z. Kristallogr. **136**, 273 (1972).

[88] J. Akimoto, Y. Gotoh, Y. Oosawa, N. Nonose, T. Kumagai, K. Aoki, and H. Takei, J. Solid State Chem. **113**, 27 (1994).

[89] R. Marchand, L. Brohan, and M. Tournoux, Mater. Res. Bull. **15**, 1129 (1980).

[90] M. Latroche, L. Brohan, R. Marchand, and M. Tournoux, J. Solid State Chem. **81**, 78 (1989).

Table I: Parameters for the various interatomic potentials used (equations 5 and 6) for molecular dynamics simulations of $TiO_2$. The three Teter parameters that were modified are italicized (see main text). The final column gives the approximate density derived after simulation in the *NPT* ensemble at 1 atm and 2243 K.

| Potential | $f$ | Pair $ij$ | $A_{ij}$ (eV) | $B_{ij}$ (Å$^{-1}$) | $\sigma_{ij}$ (Å) | $C_{ij}$ (eV Å$^{-6}$) | $D_{ij}$ (eV Å$^{-8}$) | *NPT* $\rho$ (g cm$^{-3}$) |
|---|---|---|---|---|---|---|---|---|
| Matsui & Akaogi | 0.549 | Ti-O | 78.31676 | 5.154639 | 2.8162 | 117229.7 | 0 | 1.4 |
| | | O-O | 1319.193 | 4.273504 | 3.2678 | 281351.2 | 0 | |
| Teter | 0.6 | Ti-O | 23707.91 | 5.388512 | 0 | 14.513 | 0 | 2.9 |
| | | O-O | 1844.746 | 2.90998 | 0 | 192.58 | 0 | |
| Modified Teter | 0.6 | Ti-O | 23707.91 | 5.388512 | 0 | 14.513 | *1.28* | 3.2 |
| | | O-O | *1881.641* | 2.90998 | 0 | 192.58 | *112* | |
| *This work* | 0.6 | Ti-O | 2963.489 | 4.028794 | 0 | 14.513 | -2.75 | 3.2 |
| | | O-O | 2213.910 | 2.90998 | 0 | 192.58 | -106 | |
| | | Ti-Ti | 18000.00 | 4.0 | 0 | 800.00 | -500 | |
| | | | $E_{ij}$ (eV) | $k_{ij}$ (Å$^{-1}$) | $r_{ij}$ (Å) | | | |
| Pedone *et al.* | 0.6 | Ti-O | 0.024235 | 2.254703 | 2.708943 | | | 2.6 |
| | | O-O | 0.042395 | 1.379316 | 3.618701 | | | |

Table II: Average Ti-O coordination numbers, $n_{\mathrm{TiO}}$, obtained from x-ray diffraction data on the $TiO_2$ melt (integration up to the minimum at 2.44 Å) at 2250(30) K, recovered Rutile $TiO_2$ (peak fit), and from the Rutile crystal structure. Peak (modal) bond lengths, $r_{\mathrm{TiO}}$, are also given. The corresponding values obtained from $g_{\mathrm{TiO}}(r)$ for the melt from different MD models and from EPSR are also given, where the second column gives the quality-of-fit parameter, $R\chi$ (for $r_{k,max}$ = 10 Å, equation 7), and the fourth the $n_{\mathrm{TiO}}$ obtained by integration up to the first minimum of $g_{\mathrm{TiO}}(r)$ at 2.75 Å. Uncertainties are in parentheses.

| | **$R\chi$** (%) | **$n_{\mathrm{TiO}}$** | | **$r_{\mathrm{TiO}}$ (Å)** |
|---|---|---|---|---|
| | | $r_{\mathrm{cut}}$ = 2.44 Å | $r_{\mathrm{cut}}$ = 2.75 Å | |
| Melt | - | 5.0(2) | - | 1.881(5) |
| *This work* | 2.55 | 4.71 | 5.17 | 1.87 |
| Modified Teter | 4.56 | 4.68 | 4.98 | 1.86 |
| Pedone | 6.07 | 4.40 | 4.71 | 1.82 |
| Matsui & Akaogi | 5.82 | 4.35 | 4.89 | 1.92 |
| EPSR | 0.54 | 4.82 | 5.30 | 1.87 |
| Rutile Measured | - | 5.7(2)$^a$ | 5.7(2)$^a$ | 1.962(5) |
| Rutile Ideal | - | 6.00 | 6.00 | 1.959 |

a – from peak fit, not integration

Table III: Volume thermal expansion coefficients, $\alpha_V$ (equation 8), derived from MD simulations of liquid and amorphous $TiO_2$, compared to measured values for the melt [39] and crystalline Rutile $TiO_2$ [55]. All $\alpha_V$ are referenced to $T_R$ = 298 K and the columns $\Delta T$ indicate the range over which $\alpha_V$ was calculated. Glass transition temperatures derived from the model potential energy, after Micoulaut et al. [64] are also given, as are the $T$ coefficients of $n_{\mathrm{TiO}}$ in the melt, $\mathrm{d}n_{\mathrm{TiO}}/\mathrm{d}T$.

| | **Volume thermal expansion coefficient $\alpha_V$ ($10^{-6}$ $K^{-1}$)** | | | | | | **$T_g$ (K)** | **$\mathrm{d}n_{\mathrm{TiO}}/\mathrm{d}T$ ($10^{-4}$ $K^{-1}$)** |
|---|---|---|---|---|---|---|---|---|
| | Melt | $\Delta T$ (K) | Amorphous | $\Delta T$ (K) | Rutile | $\Delta T$ (K) | | |
| MD *This work* | 81.8(7) | 1898-2798 | 30.39(2) | 298-898 | - | - | 950(110) | -3.0(1) |
| MD Mod. Teter | 70.3(7) | 1873-2743 | 27.98(2) | 298-1198 | - | - | 1330(110) | -1.7(1) |
| Measured | 89.0 [39] | 1873-2198 | - | - | 27.35 [55] | 296-1578 | - | - |

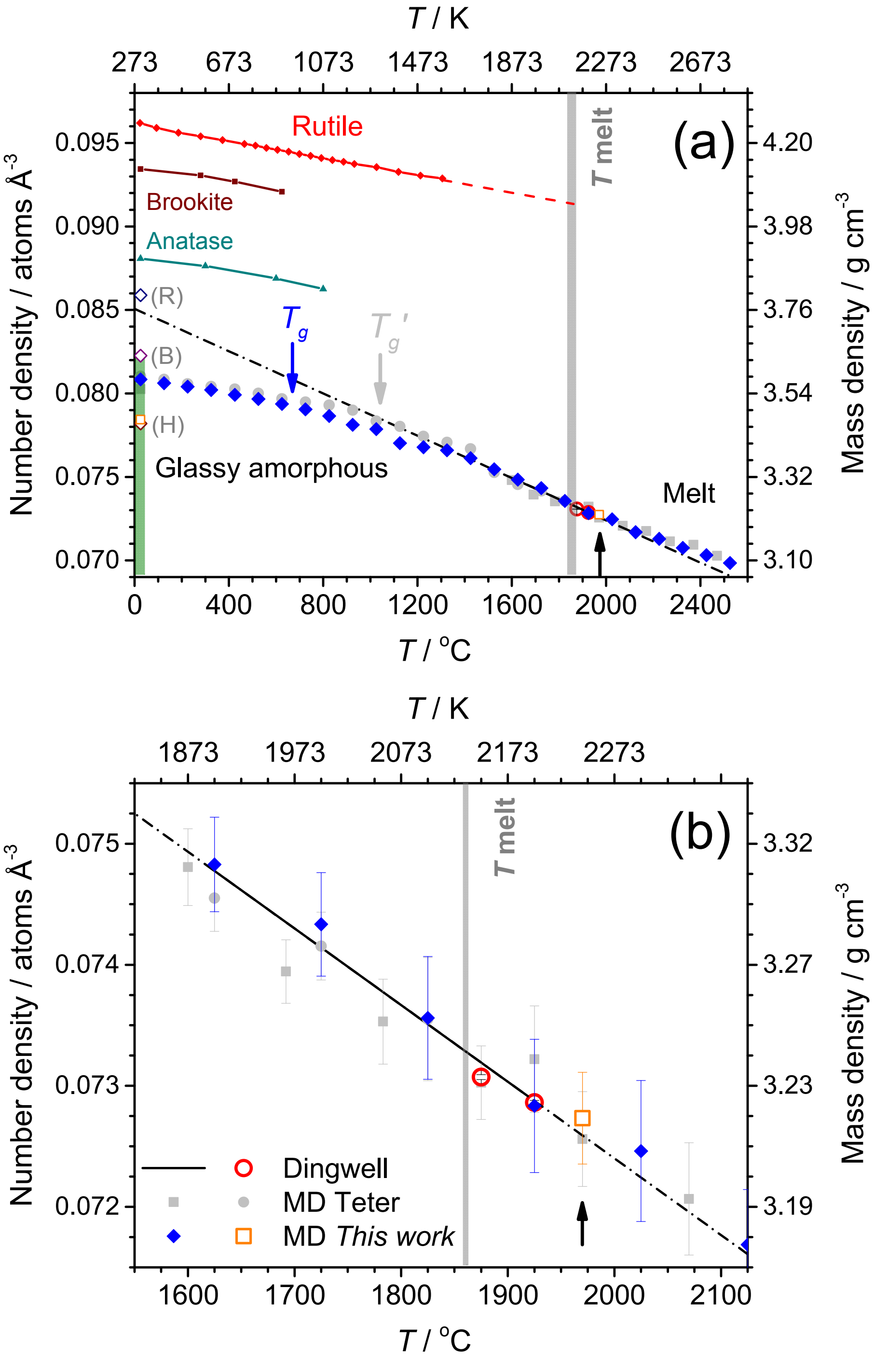

Figure 1: a) Experimental temperature dependence of the densities of Rutile [55], Brookite [86], Anatase [87] and liquid [39] $TiO_2$ (open red circles). The solid black line is the trend derived by Dingwell [39] and its extrapolation is shown as a broken dash-dot curve. The Rutile trend is extrapolated (dashed curve) up to the melting point (vertical grey bar). Points denoted (R), (B), (H) respectively show the room-temperature densities of Ramsdellite [88], Beta- [89] and Hollandite [90] $TiO_2$. The vertical green bar plots the range of room temperature densities of amorphous $TiO_2$ thin films obtained by Mergel *et*

*al*. [17]. Densities of liquid and amorphous $TiO_2$ obtained by molecular dynamics modelling using the potentials derived in this work are shown as closed (blue) diamonds and open (orange) squares, and using the modified Teter potentials; closed (grey) squares and circles (quench). Glass transition temperatures are indicated as $T_g$ and $T_g'$ respectively. The vertical black arrow indicates the temperature of the x-ray diffraction measurement (this study). Part b) shows a close up around the melting point. Error bars are standard deviations. In color online.

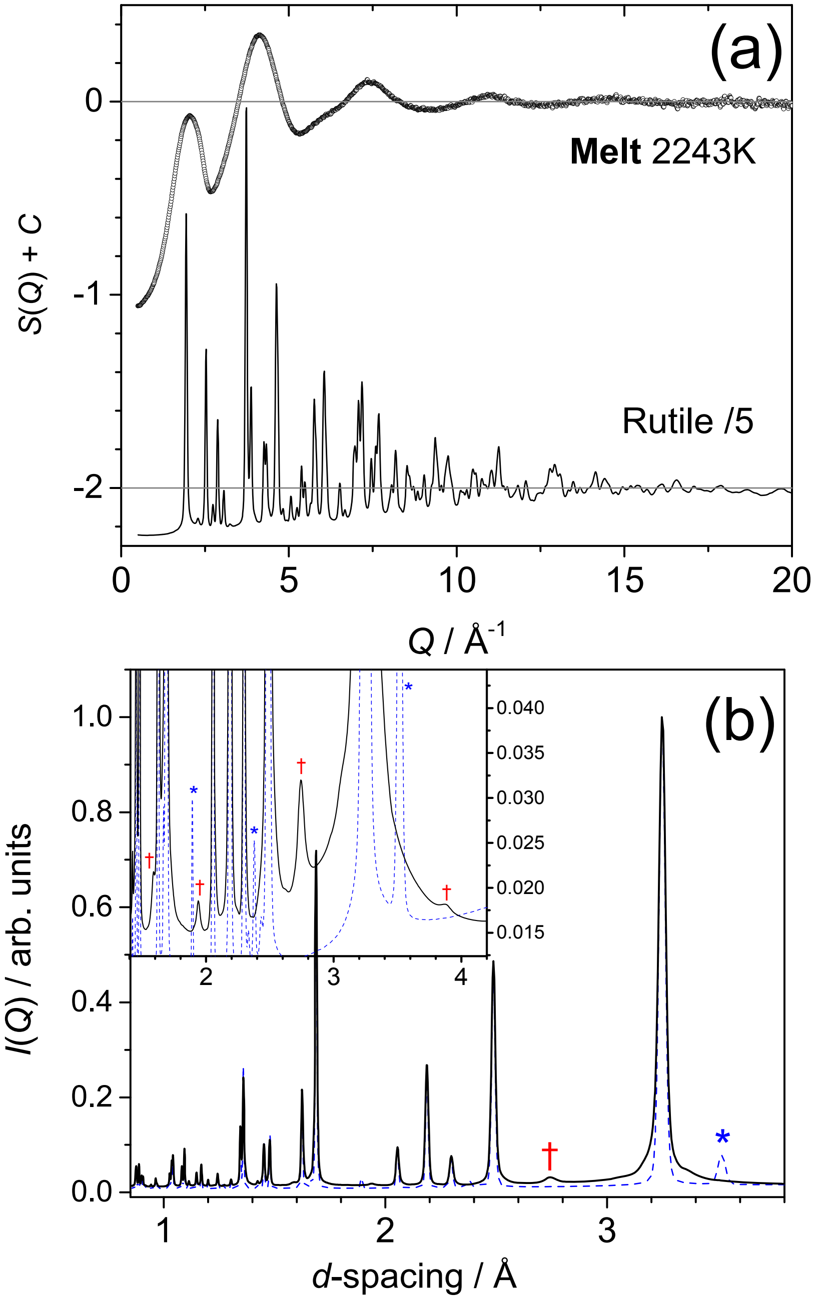

Figure 2: a) Structure factors $S(Q)$ for liquid (2250 K) and recovered Rutile $TiO_2$ , the latter has been divided by a factor 5, and constant offsets $C$ applied, for clarity. b) Higher resolution (see main text)

diffraction patterns $I(Q)$ for starting material (dashed blue curve) and recovered material (solid black curve) as functions of inter-planar spacing $d = 2\pi/Q$. Asterisks (*) denote an Anatase impurity in the predominantly Rutile starting material, while daggers (†) denote unmatched Bragg peaks of a phase impurity in the predominantly Rutile recovered material.

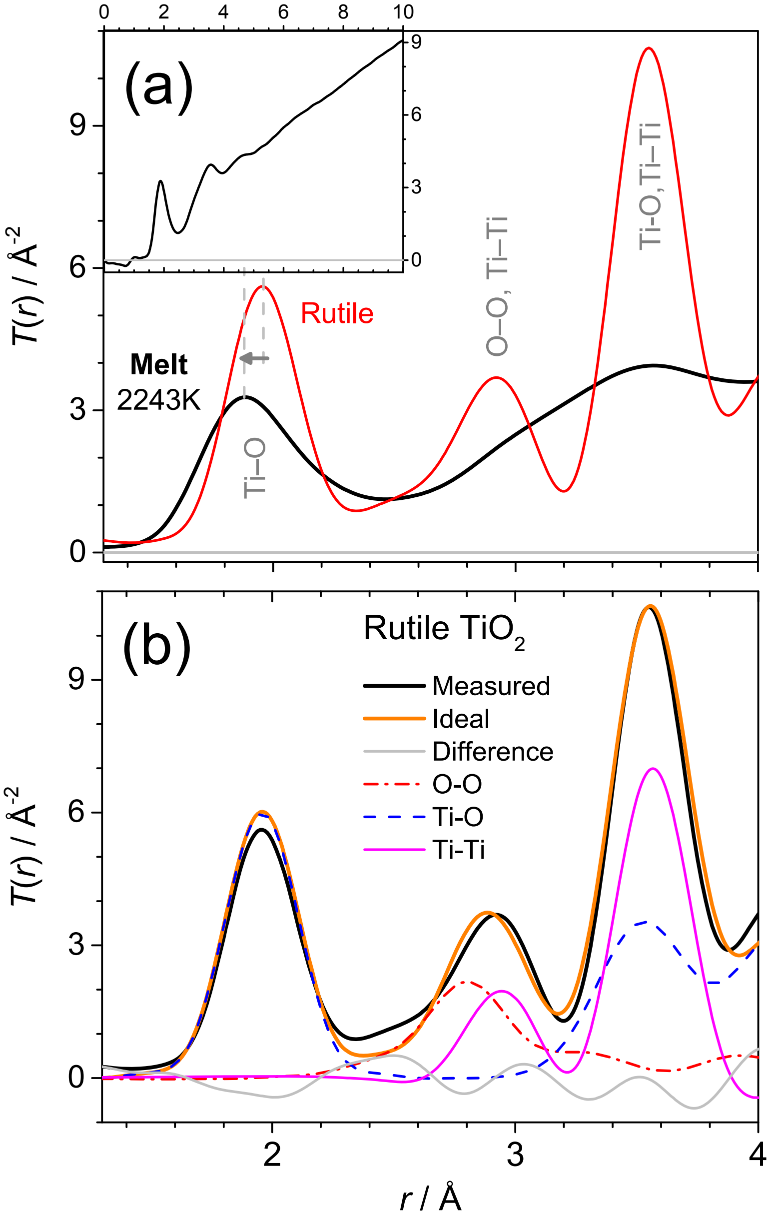

Figure 3: a) Total correlation functions $T(r)$ for the melt at 2250(30) K and the recovered Rutile $TiO_2$ at room temperature. Inset: $T(r)$ for the melt over an extended $r$ range. b) Comparison of measured and ideal Rutile $TiO_2$ $T(r)$, also showing the partial pair functions calculated from the known crystal structure. In color online.

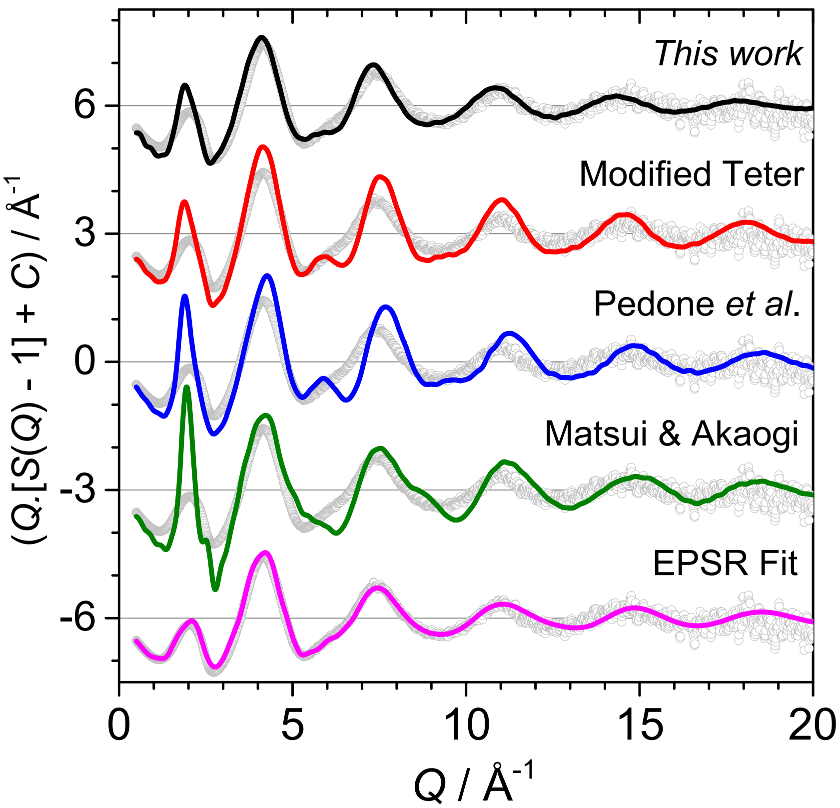

Figure 4: Interference functions *Q*(*S*(*Q*)-1) for various molecular dynamics models (solid curves) obtained using the potentials of this work (*NPT*), Teter (Modified, *NPT*), Pedone *et al*. [48] (*NVT*), Matsui & Akaogi [46] (*NVT*), compared to the experimental data (open points). A model derived by empirical potential structure refinement (EPSR) to the measured x-ray structure factor is also shown. Vertical offsets *C* have been applied for clarity.

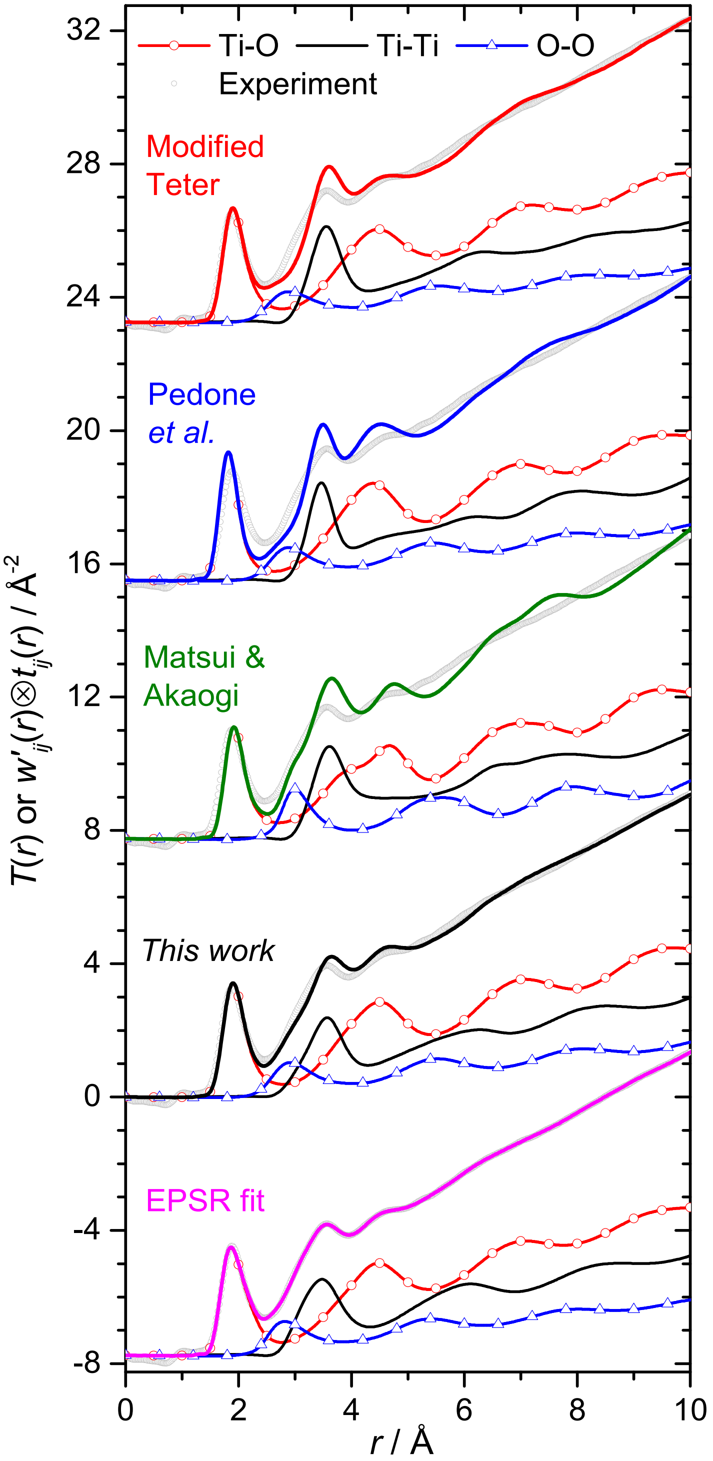

Figure 5: Comparison of experimental $T(r)$ (open points) to those from molecular dynamics modelling and EPSR, Fourier transformed from the interference functions shown in Fig. 4. Also shown are the x-ray weighted partial correlation functions $w'_{ij}(r)\otimes t_{ij}(r)$ where $w'_{ij}(r)$ are the Fourier transforms of the $W_{ij}(Q)$ (equation 3) and $\otimes$ denotes convolution. Vertical offsets have been used for clarity. In color online.

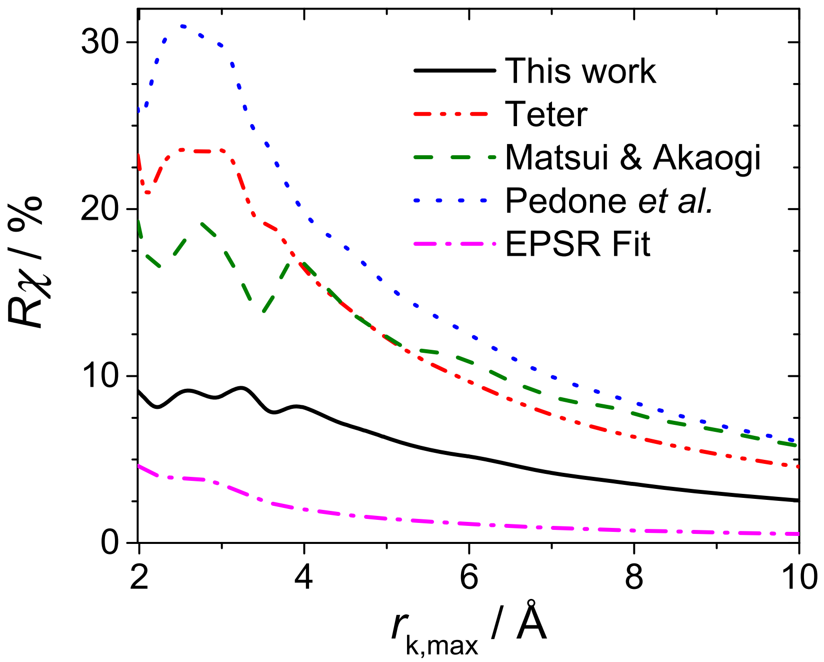

Figure 6: Dependence of the quality-of-fit parameter, $R\chi$ (equation 7), on the upper cutoff distance $r_{k,max}$ for the five molten $TiO_2$ models considered (see Fig. 5 and Table II).

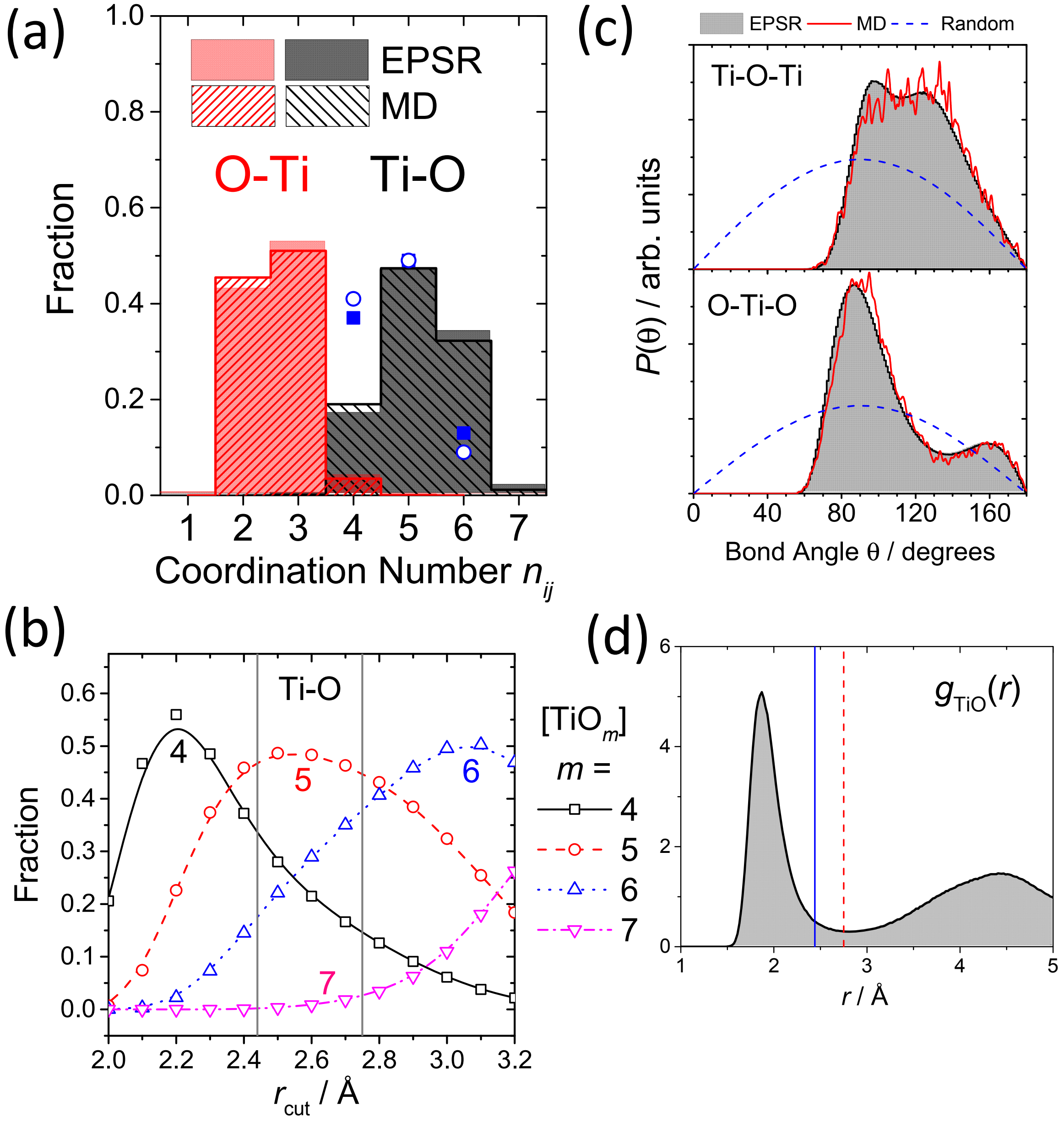

Figure 7: a) and b) coordination number and c) bond angle distributions calculated for the EPSR and modified Teter MD models of molten $TiO_2$ at 2243 K. The cutoff distance for Ti-O separations used in parts a) and c) was 2.75 Å, while b) shows the dependence of the Ti-O coordination number distribution on cutoff distance, $r_{\text{cut}}$, for the EPSR model, lines are guides to the eye. Vertical lines correspond to cutoffs used to calculate the averages in Table II, and these are also compared to $g_{\text{TiO}}(r)$ in part d). Si-O coordination number distributions for high pressure liquid silica are shown for comparison in part a) as closed blue squares (*ab initio* MD [67], 3500 K, 27 GPa) and open blue circles (*ab initio* MD [68], 3000 K, 20 GPa). In color online.

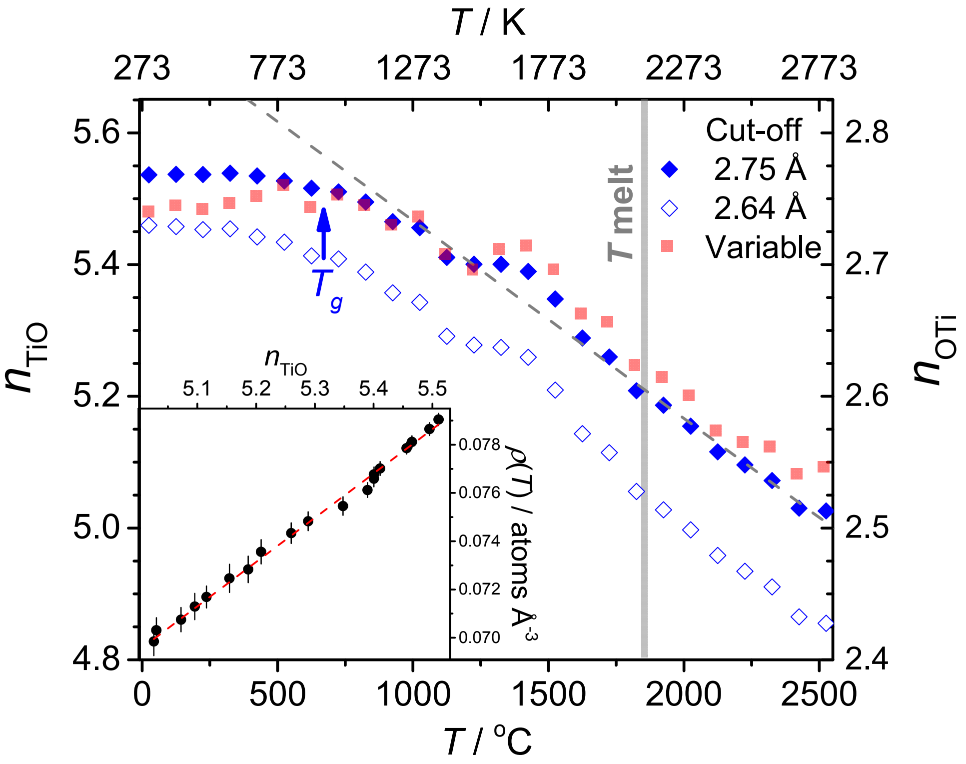

Figure 8: Average coordination numbers of liquid and amorphous $TiO_2$ obtained by molecular dynamics modelling using the potentials of this work; the glass transition temperature is indicated as $T_g$. Values for two fixed cutoffs and for a variable cutoff set at the minimum of $g_{TiO}(r)$. The right hand ordinate axis shows $n_{OTi} = (1/2)n_{TiO}$. The dashed line is a fit to the equilibrium liquid data, and its extrapolation to lower temperatures, and is given by $n_{TiO} = 5.8497 - (3.00625 \times 10^{-4})T$ (in K). Inset shows number density, $\rho(T)$, as a function of $n_{TiO}$ (2.75 Å cutoff), with the dashed (red) line a least squares fit. The cutoffs for the variable cutoff points (light red squares) were determined by 4th order polynomial fits to $g_{TiO}(r)$ in the region $2.26 < r < 3.40$ Å. In color online.

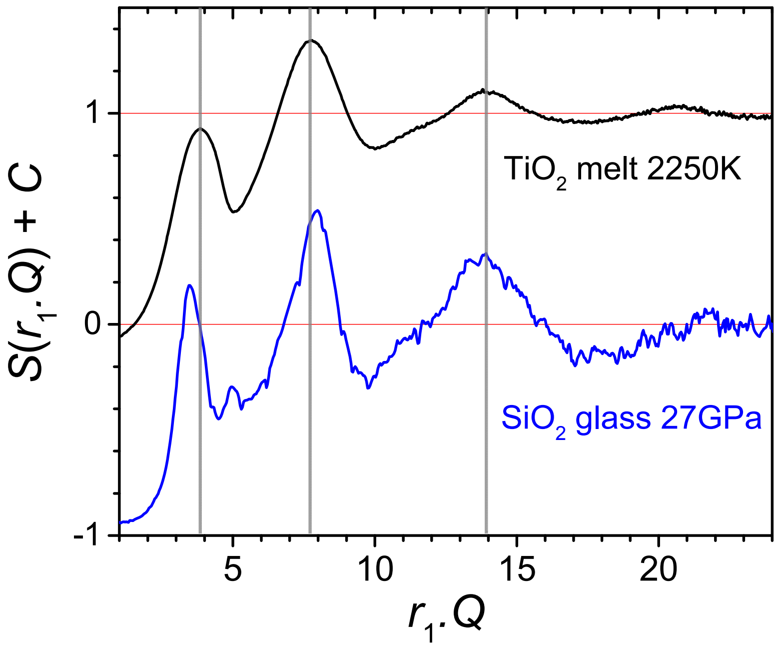

Figure 9: Comparison of the x-ray structure factors for liquid $TiO_2$ and room temperature $SiO_2$ glass at 27 GPa [66], plotted as functions of the dimensionless coordinate $r_1Q$, where $r_1$ is the peak Ti-O or Si-O bond length as measured in the Fourier transforms of the respective $S(Q) - 1$.